Chemical Science

Accepted Manuscript

Chemical Science

rsc.li/chemical-science

ISSN 2041-6539

EDGE ARTICLE
Xinjing Tang et al.
Caged circular siRNAs for photomodulation of gene
expression in cells and mice

Volume 9
Number 1
7 January 2018
Pages 1-268

ROYAL SOCIETY
OF CHEMISTRY

This is an Accepted Manuscript, which has been through the Royal Society of Chemistry peer review process and has been accepted for publication.

Accepted Manuscripts are published online shortly after acceptance, before technical editing, formatting and proof reading. Using this free service, authors can make their results available to the community, in citable form, before we publish the edited article. We will replace this Accepted Manuscript with the edited and formatted Advance Article as soon as it is available.

You can find more information about Accepted Manuscripts in the Information for Authors.

ROYAL SOCIETY
OF CHEMISTRY

rsc.li/chemical-science

Copper depletion-induced tumor cuproptosis

Min Zhou,[1#] Faheem Muhammad,[1#,5] Yihong Zhang,[1] Tong Li,[1] Jiayuan Feng,[1,4] Jingyuan Zhao,[1] Hui Wei[1,2,3]*

[1]Department of Biomedical Engineering, College of Engineering and Applied Sciences, Nanjing National Laboratory of Microstructures, Jiangsu Key Laboratory of Artificial Functional Materials, Nanjing University, Nanjing, Jiangsu 210023, China.

[2]State Key Laboratory of Analytical Chemistry for Life Science, School of Chemistry and Chemical Engineering, Chemistry and Biomedicine Innovation Center (ChemBIC), ChemBioMed Interdisciplinary Research Centre at Nanjing University, Nanjing University, Nanjing, Jiangsu 210023, China.

[3]Nanozyme Laboratory in Zhongyuan, Henan Academy of Innovations in Medical Science, Zhengzhou, Henan 451163, China.

[4]Department of Materials Engineering, Graduate School of Engineering, The University of Tokyo, Tokyo 113-8656, Japan.

[5]Guangdong Key Laboratory of Biomedical Measurements and Ultrasound Imaging, School of Biomedical Engineering, Shenzhen University Medical School, Shenzhen University, Shenzhen, Guangdong 518000, China.

#Equal contribution.

*Corresponding authors.

E-mail: weihui@nju.edu.cn.

Abstract

Copper homeostasis is crucial for cells, especially for rapidly proliferating cancerous cells. Copper imbalance-induced cell death (*i.e.*, cuproptosis) has emerged as a new strategy for tumor therapy. While copper accumulation-induced cuproptosis has been extensively investigated and its underlying mechanism recently elaborated, copper depletion-induced cuproptosis remains largely unexplored. Herein, we demonstrated copper depletion-induced tumor cuproptosis through the development of a smart

copper-depleting nanodrug (*i.e.*, ZnS nanoparticle), leveraging a cation exchange reaction between ZnS and copper ions. This cation exchange reaction is driven by the large difference in solubility product constants (K_{sp}) between ZnS and CuS. Our ZnS nanoparticle demonstrated a potent copper-depleting ability, which induced tumor cuproptosis both *in vitro* and *in vivo*. We proposed a copper-depleting mechanism primarily linked to the dysfunction of cellular copper-contained enzymes, contrasting with the mechanism of copper accumulation-induced cuproptosis. Furthermore, by modifying the ZnS nanoparticle with a polydopamine shell and a glucose transporter 1 DNAzyme (GD), we developed a multifunctional copper nanoconsumer with strong tumor growth and metastatic inhibition activity, enhancing copper depletion-promoted tumor therapy.

Introduction

Copper (Cu), an essential trace element for all organisms, participates in many biological processes, including mitochondrial respiration, redox homeostasis, and kinase signaling.[1-3] Notably, intracellular copper must be maintained in a strict range. A slight deviation from its physiological concentration can disrupt a series of cellular processes, causing diseases such as Menkes (due to copper deficiency), Wilson (due to copper accumulation), and even cancer.[4-7] Earlier studies reported that tumor cells have a higher copper content to maintain rapid proliferation,[8,9] but this content must also be controlled within an optimal range. Therefore, modulating copper level in cancer cells has emerged as a promising strategy for tumor therapy *via* either copper overaccumulation or depletion.[10-12]

To date, enormous efforts have been devoted to copper accumulation-induced cuproptosis.[13-18] Notably, copper ionophores such as elesclomol and disulfuram have been used for exogenous copper delivery. Recently, the mechanism of copper accumulation-induced cuproptosis has been elucidated, characterizing by the aggregation of lipoylated proteins and decrease of Fe-S cluster proteins, then leading to cell death.[19] However, copper accumulation inevitably requires supplementary copper ions, which has limited the wide adoption of copper accumulation-induced cuproptosis.

In contrast, copper depletion-mediated cuproptosis provides a promising strategy to tackle the aforementioned challenge by sequestering cellular bioavailable copper ions with copper chelators.[12] Among these copper chelators, several have advanced to the preclinical/clinical phase for cancer therapy, including trientine, ATN-224, and tetrathiomolybdate (TTM).[20-22] Encouragingly, TTM has already reached clinical phase II for breast cancer and has shown inhibition of tumor growth.[12,23] However, large dosages of these molecular chelators are needed to effectively sequester cellular copper, which not only cause side effects but also ultimately induce drug resistance. While nanoparticulate and polymeric systems have been developed for copper depletion, the majority still rely on the molecular chelators.[24-26] Therefore, designing new types of copper depletion independent of molecular chelators is greatly needed.

Inspired by the solubility product (K_{sp}) concept, we envisioned that mesoporous zinc sulfide (ZnS) nanospheres could be used for copper depletion through a cation exchange reaction between ZnS and copper ions, leveraging the large difference in K_{sp} of ZnS and CuS (K_{sp} of ZnS as 1.6×10^{-24} and CuS as 6.3×10^{-36}, respectively) (Table S1).[27-38] Herein, we synthesized ZnS nanoparticles for copper depletion-induced cuproptosis, which is distinct from previously reported chelators. Additionally, we proposed the copper depletion mechanism. Through further functionalization of ZnS, both primary and metastatic tumor were significantly inhibited based on copper depletion.

Results and Discussion

Synthesis and copper depleting ability of ZnS

Based on an organic–inorganic interaction mode, mesoporous ZnS nanospheres were synthesized by a ligand-assisted metal coordination strategy.[39-41] Typically, zinc nitrate as a metal source, thioacetamide (TAA) as a sulfur source, citric acid (CA) and hexamethylene tetramine (HMTA) as ligands, and cetyltrimethylammonium bromide (CTAB) as a template, these agents reacted together to produce ZnS nanospheres (Fig. 1a). The morphology of ZnS was determined through a transmission electron microscope (TEM), showing a mesoporous-spherical structure with a size of about

97±4 nm (Fig. 1b). The hydrodynamic size and dispersity of the ZnS were measured by dynamic light scattering (DLS), showing a size of about 164 nm and good dispersity (polydispersity index, PDI=0.107) (Fig. 1c).
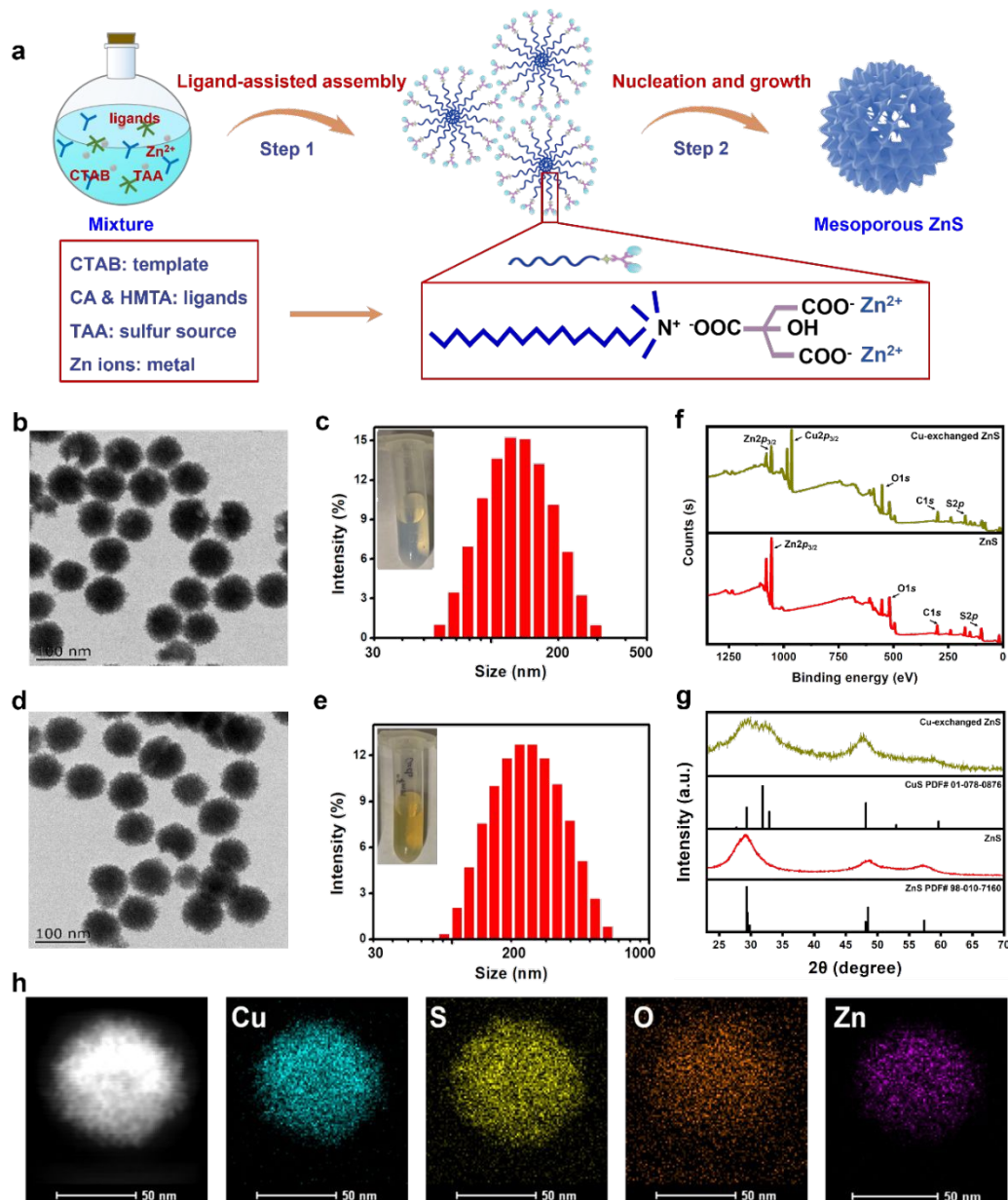
Figure 1. Characterization and copper depleting ability of ZnS. (a) Schematic of mesoporous ZnS nanosphere synthesis. (b) TEM image of ZnS. (c) Size distribution of ZnS. Inset: digital photo of ZnS solution. (d) and (e) TEM image and size distribution of Cu-exchanged ZnS by TEM and DLS. Inset: digital photo of ZnS after Cu depletion. (f) XPS analysis of ZnS and Cu-exchanged ZnS. (g) XRD patterns of ZnS and Cu-exchanged ZnS. (h) Element distribution mapping of ZnS after Cu depletion by HRTEM.

Given the disparity in K_{sp} values between ZnS and CuS, we envisioned that the ZnS could exchange with Cu^{2+} and produce CuS (Fig. S1). To test this, we explored the

cation-exchanging ability of ZnS by adding Cu^{2+} ($CuCl_2$ as the donor of Cu^{2+}) to the ZnS solution. Gradually increasing amounts of Cu^{2+} were dropwise added into ZnS solution (20 μg/mL ZnS). An obvious color change of the reaction solution from ivory-white (ZnS, inset photo in Fig. 1c) to yellowish green (Cu-exchanged ZnS, inset photo in Fig. 1e) was observed. The products were harvested and analyzed for copper and zinc content using inductively coupled plasma-optical emission spectrometry (ICP-OES). The results revealed that the copper stack proportion (compared with Zn) increased in a Cu^{2+} concentration-dependent manner and reached to 98% when 30 μM Cu^{2+} was added (final concentration, in 20 μg/mL ZnS solution) (Fig. S2), thus verifying the copper-exchanging ability of ZnS. When higher concentrations of Cu^{2+} were supplemented, a plateau of copper proportion was observed. This was probably due to the saturation point beyond which Zn could not be exchanged with the remaining Cu^{2+}. Then, we characterized the Cu-exchanged ZnS product (final concentration, 30 μM Cu^{2+} exchanging with 20 μg/mL ZnS). It exhibited similar morphology and size to that of ZnS in the TEM image (Fig. 1d) and good dispersity determined by DLS (Fig. 1e). These results indicated the occurrence of cation exchange.

Subsequently, X-ray photoelectron spectroscopy (XPS) was performed to determine the composition of ZnS and Cu-exchanged ZnS. The Cu $2p$ peak emerged while the intensity of the Zn $2p$ peak decreased (using the peak of S $2p$ as an internal reference) in the Cu-exchanged ZnS (Fig. 1f). The powder X-ray diffraction (XRD) analysis indicated the crystalline phase of Cu-exchanged ZnS with peaks consistent with CuS (PDF card No: 01-078-0876) (Fig. 1g), confirming the formation of CuS through a cation exchange reaction. High-resolution TEM (HRTEM) and energy-dispersive X-ray spectroscopy (EDS) elemental mapping revealed a homogenous distribution of Cu and S elements in the produced CuS, with a smaller portion of Zn content. This result was consistent with the earlier observation that cation exchange has a saturation point that prevents further Cu^{2+} exchange (Fig. S2). Semiquantitative EDS analysis was also performed, showing that the weight content of Cu (4.99%) and Zn (1.33%) in produced CuS, compared with 5.62% Zn in ZnS (Fig. S3). These findings were mutually consistent, confirming the copper-exchanging ability of ZnS and the

formation of CuS. Therefore, we hypothesized that ZnS could be used as a powerful copper-depleting agent for copper depletion therapy.
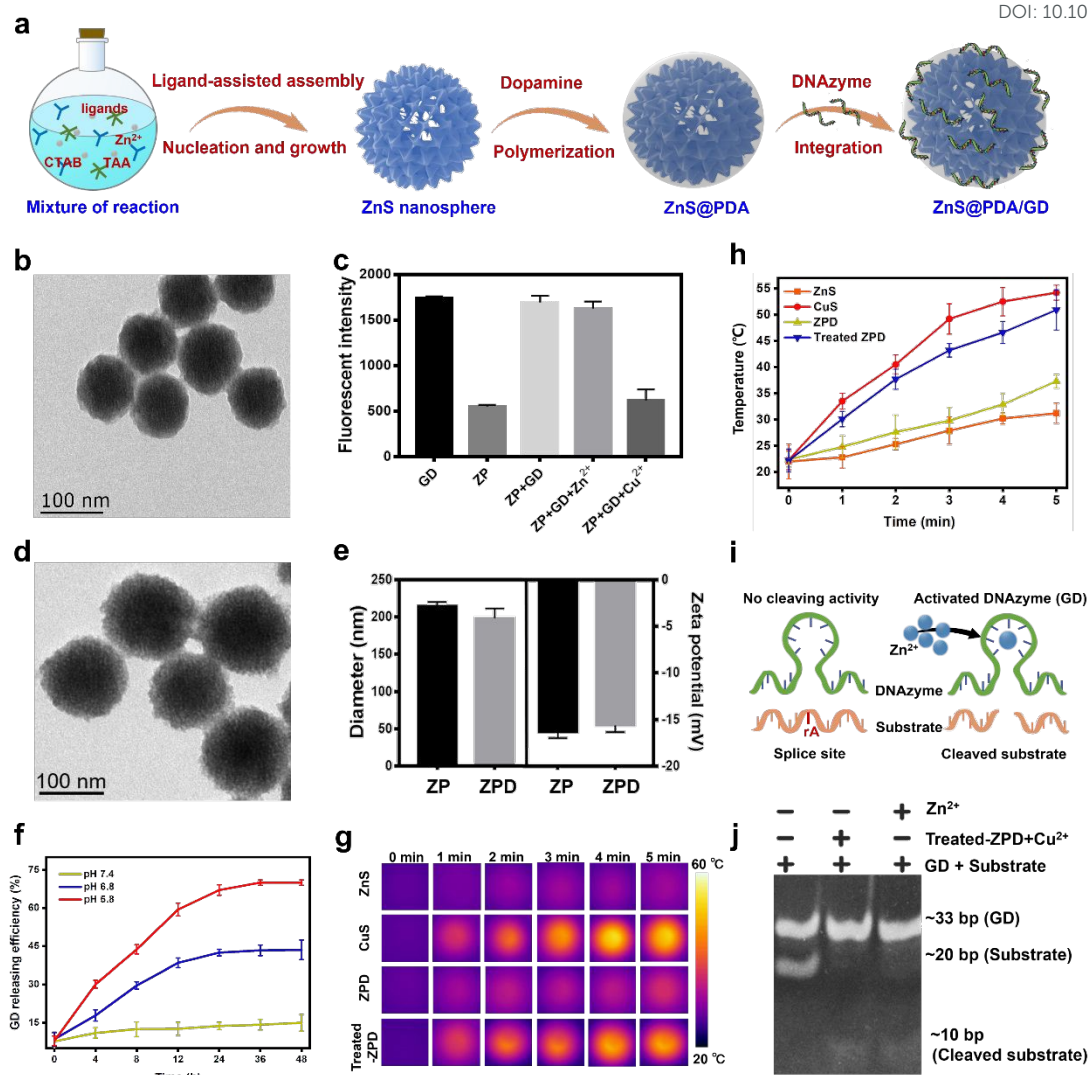
Fabrication of "copper nanoconsumer"

To facilitate targeted copper depletion, a "copper nanoconsumer" was fabricated by functionalizing the surface of ZnS (Fig. 2a). A thin shell of polydopamine (PDA), a bio-inspired acid-degradable material widely applied for surface coating,[42,43] was polymerized on the ZnS for core protection, obtaining ZnS@PDA (termed ZP). It has been reported that cellular copper depletion could induce mitochondrial dysfunction, shifting cancer cells metabolism more to glycolysis. [7,8,44] Therefore, we designed a Zn^{2+} dependent glucose transporter 1 (Glut 1) mRNA-cleaving DNAzyme (*i.e.*, GD) for selective glycolytic inhibition.[45-47] Finally, GD was conjugated on ZP *via* a metal ion assisted DNA adsorption strategy,[48,49] ZnS@PDA/GD (termed ZPD) as the "copper nanoconsumer" was obtained.

The monodispersed core-shell structure of ZP was demonstrated by TEM imaging (Figs. 2b), showing a thickness of PDA shell about 3 nm. The successful conjugation of GD was confirmed by fluorescent quenching analysis and gel electrophoresis(Figs. S4 and S5). The GD loading efficiency in ZPD was up to 79.34% by fluorescent measurement (Fig. 2c). The ZPD was characterized by TEM imaging (Fig. 2d), size distribution (Fig. S6), and elemental mapping analysis (Fig. S7), showing a similar morphology as ZP with a small change in the hydrodynamic diameter and zeta potential (Fig. 2e). These results demonstrated the successful synthesis of ZPD.

Figure 2. Synthesis and characterization of "copper nanoconsumer" ZPD. (a) Scheme of "copper nanoconsumer" synthesis. (b) TEM image of ZP. (c) Metal ion-mediated adsorption between ZP and GD, probed by fluorescence quenching analysis. (d) TEM image of ZPD. (e) Comparison of diameters and zeta potentials between ZP and ZPD by dynamic light scattering. (f) GD release profile at different pHs. (g) Photothermal imaging under laser irradiation, 808 nm 2 W/cm² for 5 min. (h) Photothermal effect analysis by monitoring temperature changing under laser irradiation. 808 nm 2 W/cm² for 5 min. (i) Schematic description of DNAzyme-mediated mRNA cleavage. (j) Gel electrophoresis of GD cleaving activity. Each error bar represents the standard deviation of four independent measurements.

Subsequently, the properties of ZPD were explored. First, the degradation of PDA was monitored by treating ZPD (Cy3-labeled GD) in different pH buffers (20 mM phosphate buffer, pH=7.4, 6.8, and 5.8). When ZPD was treated with pH 5.8 buffer (termed treated-ZPD), the highest GD release efficiency was achieved, as indicated by fluorescent recovery (Fig. 2f). Degradation of the PDA shell was also observed by TEM

imaging (Fig. S8). Both results verified PDA degradation under acidic conditions, similar to the acidic microenvironment in tumors. Second, after PDA degradation, the "naked" ZnS could mediate copper depletion and CuS could be produced *in situ*. With the photothermal effect of CuS, an apparent temperature increase was noticed under laser irradiation (808 nm laser, 2W/cm^2 at different time points) in the treated-ZPD group by adding Cu^{2+}, while the ZPD group showed a weak temperature rise due to the protection of the PDA shell (Fig. 2g and 2h). These results demonstrated that after PDA degradation, ZnS-mediated cation exchange could occur in the presence of Cu^{2+} and produce photothermal active CuS. Third, the released Zn^{2+} during the copper-cation exchange reaction could specifically activate the cleaving ability of GD DNAzyme (Fig. 2i). As shown in Fig. 2j, both GD+substrate with treated-ZPD+Cu^{2+} group and GD+substrate with Zn^{2+} group could successfully cleave the substrate, whereas no cleaved substrate was noticed in only GD+substrate group. Our findings demonstrated the occurrence of ZnS-mediated copper depletion and GD activation by the released Zn^{2+} ions.

Copper depletion by ZPD at cellular level

Copper is usually associated with cancer development, and cancerous cells typically accumulate more copper to support rapid proliferation.[11,50-52] To confirm this phenomenon, we measured cellular Cu content with and without Cu supplementation in culture medium. As shown in Fig. 3a, in 4T1 tumor cells, copper content increased by 3.6-fold with copper addition (about 5.4 fg/cell) compared to the one without supplementation (about 1.5 fg/cell), whereas there was no obvious change in normal L02 cells after Cu supplementation for 24 h. Prolonging the incubation time with copper to 48 h and 72 h showed similar trends, with increased copper uptake observed in 4T1 cells after copper addition (Fig. S9). Meanwhile, copper content in other cancerous cells was also detected, and the same phenomenon was observed, with more copper content after Cu supplementation (Fig. S10).

Given the higher copper accumulation within cancer cells and the copper-depleting property of ZPD *in vitro*, we explored its performance at cellular level. ZPD

exhibited the dose-dependent cytotoxicity for cancerous cells, but had no obvious influence on normal cells (Figs. 3b and S11). We inferred that the cytotoxicity towards cancerous cells was associated with ZPD-mediated copper depletion. To validate the occurrence of cellular copper depletion, high-angle annular dark-field scanning transmission electron microscopy (HAADF-STEM) imaging and elemental mapping were performed. Greater Cu was observed in locations of endocytosed-nanoparticles, demonstrating Cu-ZnS exchange-mediated cellular copper depletion (Fig. 3c). In contrast, the distribution of Cu was uniform in untreated cells (Fig. S12), further implying ZPD-mediated cellular copper depletion. Cellular copper depletion is associated with mitochondrial dysfunction.[7,8,44] Bio-TEM shed light on this process. As shown in Fig. 3d, ZPD was successfully endocytosed by 4T1 cells and mitochondrial damage was clearly observed. Because of mitochondrial damage, the oxygen consumption rate (OCR), as an indicator of mitochondrial respiration, was monitored using a Seahorse XFe96 analyzer. 4T1 cells were co-incubated with ZnS, ZP, and ZPD. As shown in Fig. 3e, basal respiration and maximal respiration were reduced in each treated group compared to the untreated one, corroborating the copper depletion phenomenon.

Mechanism of copper depletion by ZPD

Having demonstrated the cellular copper depletion by ZnS, we further explored its mechanism. The mechanism of copper overaccumulation-mediated cuproptosis is characterized by the aggregation of lipoylated protein and decrease of Fe-S cluster proteins.[19] Therefore, we analyzed the expression of DLAT (dihydrolipoamide S-acetyltransferase, as one indicator of lipoylated protein) and FDX1 (ferredoxins, as a family of Fe-S cluster proteins) by western blotting (Fig. 3f)., There was no obvious discrepancy for these two proteins' expression, which were obviously changed in copper-accumulated cuproptosis with DLAT aggregation and FDX1 decrease. We conjectured that the mechanism of copper-depleting cuproptosis should be different from the overaccumulation mechanism. To get further insights into the copper depletion mechanism, cellular transcriptomic analysis was carried out. ZnS, ZP, and ZPD showed

different transcripts per million (*e.g.*, TPM) compared to the control group (Fig. S13). In contrast, TPM of DLAT and Fe-S clusters showed no significant change compared to the control group (Fig. S14). These results further indicated distinct mechanisms between copper depletion and overaccumulation.

Ceruloplasmin (*e.g.*, CP), the predominant carrier of copper, has been regarded as an indicator of copper depletion.[12,53,54] TPM of CP in "copper nanoconsumers" was significantly lower than in the control group (Fig. 3g), suggesting a cellular deficiency of available copper. Copper is an essential cofactor for important antioxidant enzymes, such as Cu/Zn superoxide dismutase (SOD1), copper chaperone for superoxide dismutase (CCS), antioxidant 1 copper chaperone (ATOX1), cytochrome *c* oxidase assembly protein 17 (COX17), and LACC1 (laccase (multicopper oxidoreductase) domain containing 1).[2,3,12] Once copper is depleted in cells, the function of these copper-containing enzymes would likely be impaired. TPM of these metalloenzymes was investigated (Fig. 3g). Four enzymes (*i.e.*, SOD1, ATOX1, COX17, and LACC1) exhibited an obvious decrease in TPM, especially for ZPD group. Because of lowered TPM of antioxidant enzymes, cellular ROS increased (Fig. S15), consequently deactivating SOD1 and decreasing GSH level (Fig. S16), particularly in the ZPD group. These phenomena were similar to the reported performance of copper-chelator DC_AC5[55].

We further carried out gene function classification by GO (gene ontology) enrichment analysis for ZPD (Figs. S17 and S18). To our surprise, the ZPD treatment was strongly associated with a series of cellular stress responses, including not only "detoxification of inorganic compound" and "stress response to metal ion" but also "detoxification of copper ion" and "stress response to copper ion" (highlighted in the red squares). We speculated that these observations were associated with copper depletion. Taken together, it is reasonable to state that ZPD could deplete and sequestrate copper ions, leading to the dysfunction of copper-containing metalloenzymes and disruption of cellular homeostasis, ultimately promoting cell death. We illustrated the possible steps of the ZPD depleting/sequestrating cellular copper in

Fig. 3h.
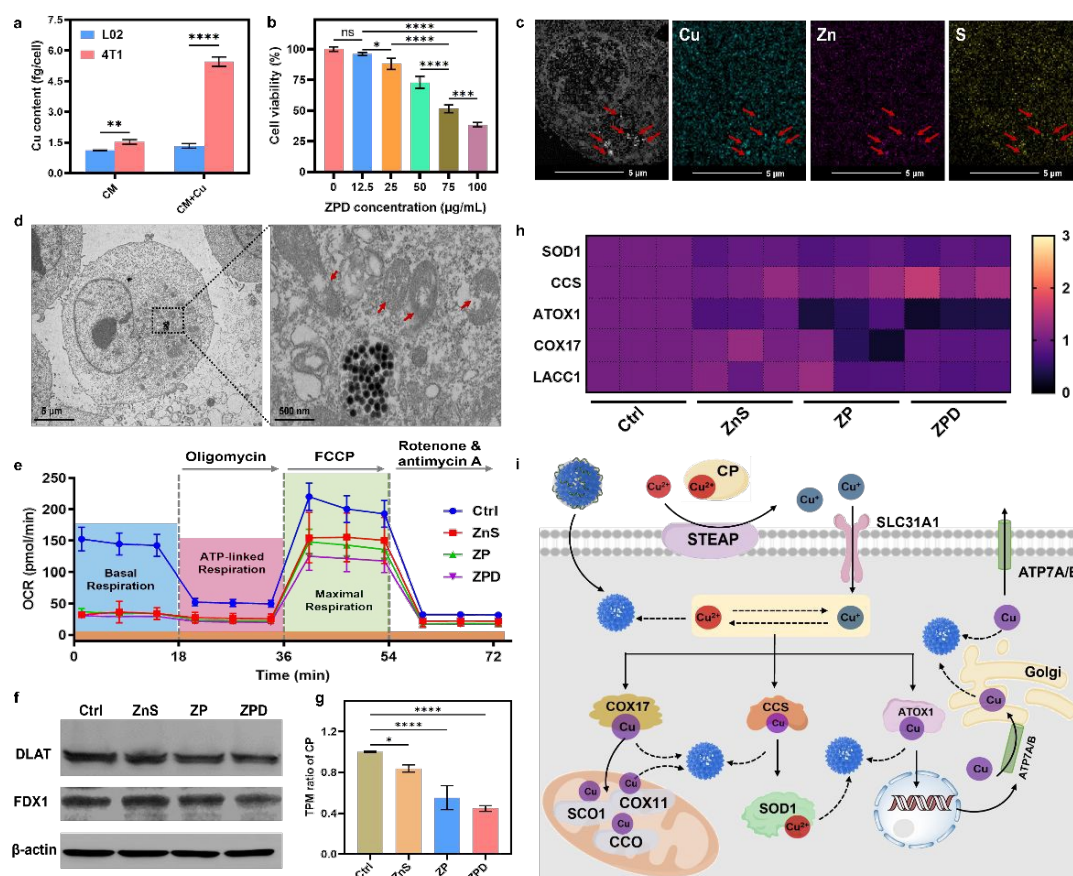
Figure 3. Cellular copper depletion by "copper nanoconsumer" ZPD and mechanistic analysis. (a) Cellular copper content with/without copper supplement in culture medium. (b) Cell viability analysis of ZPD at different concentrations in 4T1 cells. (c) HAADF-STEM and elemental mapping ZPD-treated 4T1 cell. Red arrows indicate the position of endocytosed nanoparticles. (d) Bio-TEM analysis of ZPD-treated 4T1 cells. Red arrows indicate the damage of mitochondria. (e) Analysis of mitochondrial respiration by oxygen consumption rate (OCR). (f) Western blotting analysis of DLAT expression. (g) Transcripts per million (TPM) of ceruloplasmin (CP) in different treatments. (h) Heat map of TPM in copper-associated metalloenzymes including SOD1 (Cu/Zn superoxide dismutase), CCS (copper chaperone for superoxide dismutase), ATOX1 (antioxidant 1 copper chaperone), COX17 (cytochrome c oxidase assembly protein 17), and LACC1 (laccase (multicopper oxidoreductase) domain containing 1). (i) Possible steps of copper-depleting/copper-sequestrating in cells. SOD1, Cu/Zn superoxide dismutase; CCS, copper chaperone for superoxide dismutase; ATOX1, antioxidant 1 copper chaperone; COX11, cytochrome c oxidase assembly protein 11; COX17, cytochrome c oxidase assembly protein 17; STEAP, belongs to SLC31A1 solute carrier family 31 member 1, as metalloreductases; CCO, cytochrome c oxidase; SCO1, synthesis of cytochrome c oxidase 1; ATP7A/B, for copper transporter. Solid lines: established pathways; dashed lines: proposed pathways without known mechanisms. Each error bar in a and b represents the standard deviation of four independent measurements, in e represents the standard deviation of twenty independent measurements, and in g represents the standard deviation of three independent measurements. Ordinary one-way ANOVA was used for discrepancy analysis (*P<0.05, **P<0.01,

***P<0.001, ****P<0.0001).

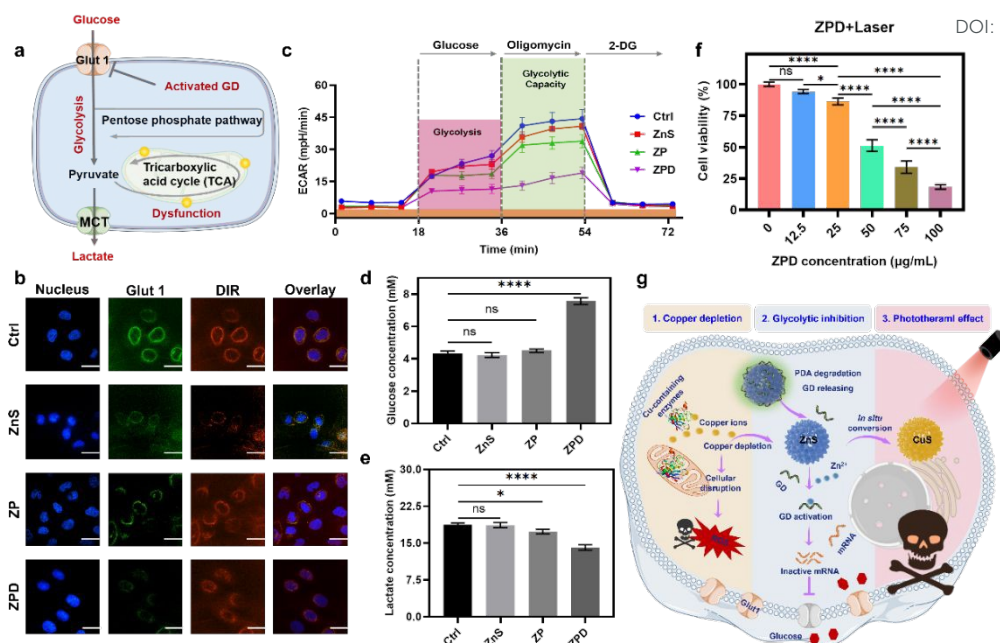## Copper depletion induces glycolytic inhibition and enables photothermal effect

As demonstrated above, the copper depletion by ZPD disrupted mitochondrial respiration and consequently shifted cells more to glycolysis. Moreover, the GD conjugated onto ZPD could be specifically activated by cation exchange-released Zn^{2+}, which would downregulate the expression of Glut 1 and further induce glycolytic inhibition (Fig. 4a). To demonstrate this hypothesis, Glut 1 expression was monitored by confocal imaging. As shown in Fig. 4b, fluorescent intensity of Glut 1 was notably downregulated in ZPD group, which was also identified by Glut 1 western blotting analysis (Fig. S19). Then, glycolytic function was measured by the extracellular acidification rate (ECAR) using a Seahorse analyzer. As shown in Fig. 4c, ZPD group exhibited the lowest glycolysis and glycolytic capacity due to GD introduction, while ZnS and ZP groups showed slightly levels lower than the control group. To further validate glycolytic inhibition, glucose and lactate content in the culture supernatant were monitored. Glucose content in the ZPD-treated culture supernatant was higher than in other groups (Fig. 4d), indicating less glucose uptake. Lactate, a product of glycolysis, was decreased in the treated culture supernatant (Fig. 4e), indicating the glycolytic inhibition, especially in the ZPD-treated group. These results were consistent and demonstrated that ZPD could induce glycolytic inhibition.

Besides Zn^{2+} releasing after copper depletion, the photothermally active CuS was formed. Therefore, the photothermal effect was evaluated by irradiating ZPD-treated cells with an 808 nm laser at a power of 2 W/cm^2 for 5 min. Greater cell growth inhibition was achieved in the laser irradiation groups (Fig. 4f) compared to those without laser irradiation (Fig. 3b). Taken together, we concluded that the "copper nanoconsumer" ZPD could perform multifunctional roles such as copper depletion, glycolytic inhibition, and photothermal effect (Fig. 4g), all of which would be significant for tumor synergetic therapy.

Figure 4. Copper depletion induces glycolytic inhibition and enables photothermal effect. (a) Schematic of glycolytic inhibition. (b) Analysis of Glut 1 expression after indicated treatments by confocal imaging. Scale bar: 5 μm. (c) Analysis of glycolytic capacity by extracellular acidification rate (ECAR). (d) and (e) Glucose and lactate content in culture supernatant after different treatments. (f) Cell viability after treatment with different concentrations of ZPD with laser irradiation (808 nm, 2 W/cm^2 for 5 min). (g) Schematic of "copper nanoconsumer" ZPD's multifunctionalities. Each error bar in c represents the standard deviation of twenty independent measurements, in d, e, and f represent the standard deviation of four independent measurements. Ordinary one-way ANOVA was used for discrepancy analysis (*P<0.05, **P<0.01, ***P<0.001, ****P<0.0001).

Anti-primary and metastatic tumor ability of ZPD

After the cellular studies, we subsequently evaluated the anti-tumor ability of ZPD *in vivo*. A subcutaneous 4T1 breast tumor model was constructed for different treatments (Fig. 5a). First, the biocompatibility was investigated by monitoring mouse weight changes (Fig. S20) and histopathological staining of major organs (Fig. S21). These results suggested no obvious side effects, demonstrating the good biosafety of nanoparticles, including ZPD. Furthermore, the biodistribution of Cu, Zn, and S with and without ZPD treatment was analyzed. As shown in Fig. S22, the levels of Zn and S increased in the ZPD-treated group, especially in tumor areas, suggesting that ZPD could accumulate in tumor areas. Although liver demonstrated the highest content of Zn and S, this was rational due to function of liver and consistent with other nanomaterials' biodistribution.[56,57]
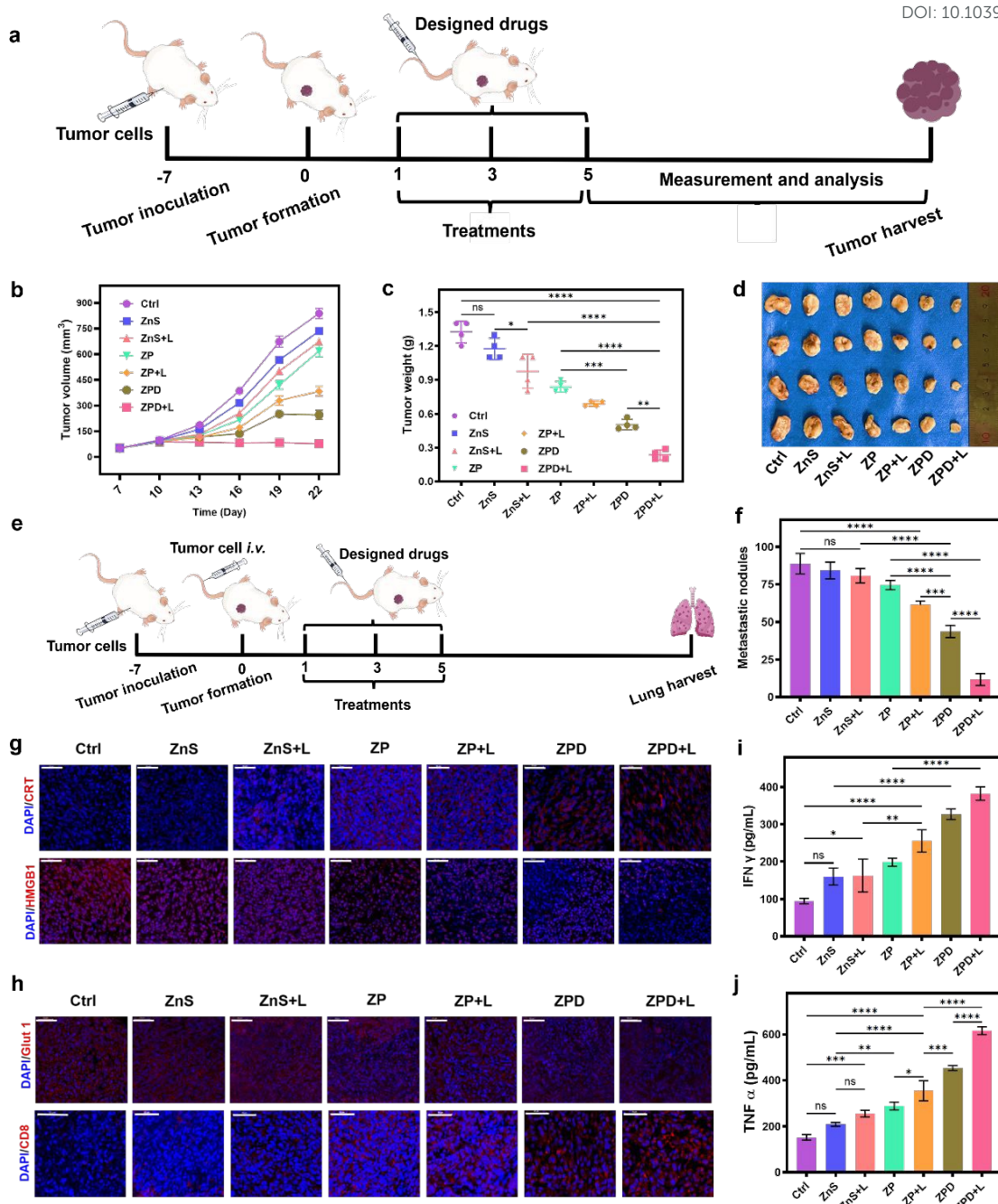
Figure 5. Anti-primary tumor and anti-metastatic ability analysis. (a) Schematic of anti-primary tumor model construction and treatment. (b) Tumor volume changes over time. (c) Tumor weight analysis by groups. (d) Tumor images by groups. (e) Schematic of constructing the lung metastasis mouse model and treatment. (f) Statistical analysis of metastatic nodules in groups. (g) Immunofluorescence analysis of ICD molecules. (h) Immunofluorescence analysis of Glut 1 expression and CD8^{+} T cell infiltration. Cytokine detection of IFN-γ (i) and TNF-α (j). All designed drugs with intravenous injection at dosage of 5 mg/kg per mouse. 808 nm laser with power of 2 W/cm² and 5 min for laser irradiation groups. Each error bar represents the standard deviation of four independent measurements. Ordinary one-way ANOVA was used for discrepancy analysis (*$P<0.05$, **$P<0.01$, ***$P<0.001$, ****$P<0.0001$). Scale bar: 50 μm.

Second, the tumor volume and weight were monitored to evaluate therapeutic efficacy (Figs. 5b-d). Without laser irradiation, anti-tumor ability was shown as ZnS<ZP<ZPD. With laser irradiation, anti-tumor ability had a similar trend as ZnS+L<ZP+L<ZPD+L, with the ZPD+L group exhibiting the greatest anti-tumor performance. To demonstrate the broad applicability, the anti-metastatic ability of our nanoparticles was also evaluated (Figs. 5e-f and S23). The trend of anti-metastatic ability among the designed groups was consistent with the anti-tumor performance. For mechanistic exploration of metastatic inhibition, we assumed that immunity may play a key role. Therefore, molecules of immunogenic cell death (ICD) such as CRT (calreticulin) and HMGB1 (high mobility group protein 1) were detected by immunofluorescent analysis (Figs. 5g and S24). The ZPD+L group demonstrated the highest CRT exposure and HMGB1 release. Additionally, Glut 1 expression decreased in the ZPD and ZPD+L groups (Figs. 5h and S25), which also benefited the immunotherapy. Immunofluorescent analysis of CD8^{+} T cell infiltration was also performed (Fig. 5h). The ZPD+L group showed the highest CD8^{+} T cell infiltration. Meanwhile, both IFN-γ (interferon γ) (Fig. 5i) and TNF-α (tumor necrosis factor α) (Fig. 5j), as important cytokines in peripheral blood of mouse, exhibited the highest levels in the ZPD+L group, demonstrating the immunotherapeutic potential. Overall, it was demonstrated that the "copper nanoconsumer" ZPD could successfully deplete cellular copper and therefore promote tumor therapy.

Conclusion

In summary, to address the challenges of copper overaccumulation-mediated tumor cuproptosis, we demonstrated copper depletion-induced cuproptosis using the "copper nanoconsumer". Unlike molecular copper chelators, the copper-depleting principal of our design was inspired by large deferent K_{sp} values between ZnS and CuS, which could promote a cation reaction between ZnS and copper ions and mediate copper depletion. Our "copper nanoconsumer" exhibited good efficacy against both primary and metastatic tumors. Additionally, the mechanism of copper depletion-induced cuproptosis was proposed, which was mainly associated with dysfunction of copper-

contained metalloenzymes. Furthermore, we investigated the representative copper-based therapies (Table S2). Although some copper-based molecular drugs were in preclinical or clinical phases, due to their intrinsic shortcomings, further efforts are needed to advance copper-based tumor therapies.[11,16,22,25,26,58-64] We envision that the copper depletion-induced tumor cuproptosis provides an alternative way for tumor therapy. Furthermore, by exploring the physiochemical characteristics of nanodrugs, more innovative therapeutics can be designed.

Acknowledgments

Conflict of interest

The authors declare no conflict of interest.

References

[1] Festa, R. A.; Thiele, D. J. Copper: an essential metal in biology. *Current Biology* **2011**, *21*, R877.

[2] Wong, P. C.; Waggoner, D.; Subramaniam, J. R.; Tessarollo, L.; Bartnikas, T. B.; Culotta, V. C.; Price, D. L.; Rothstein, J.; Gitlin, J. D. Copper chaperone for superoxide dismutase is essential to activate mammalian Cu/Zn superoxide dismutase. *Proceedings of the National Academy of Sciences of the United States of America* **2000**, *97*, 2886.

[3] Mick, D. U.; Fox, T. D.; Rehling, P. Inventory control: cytochrome *c* oxidase assembly regulates mitochondrial translation. *Nature Reviews Molecular Cell Biology* **2011**, *12*, 14.

[4] Guthrie, L. M.; Soma, S.; Yuan, S.; Silva, A.; Zulkifli, M.; Snavely, T. C.; Greene, H. F.; Nunez, E.; Lynch, B.; De Ville, C.; Shanbhag, V.; Lopez, F. R.; Acharya, A.; Petris, M. J.; Kim, B.-E.; Gohil, V. M.; Sacchettini, J. C. Elesclomol alleviates Menkes pathology and mortality by escorting Cu to cuproenzymes in mice. *Science* **2020**, *368*, 620.

[5] Walshe, J. Wilson's disease. *The Lancet* **2007**, *369*, 397.

[6] Danks, D.; Campbell, P.; Walker-Smith, J.; Stevens, B.; Gillespie, J.; Blomfield, J.; Turner, B.

Menkes' kinky-hair syndrome. *The Lancet* **1972**, *299*, 1100.

[7] Ramchandani, D.; Berisa, M.; Tavarez, D. A.; Li, Z.; Miele, M.; Bai, Y.; Lee, S. B.; Ban, Y.; Dephoure, N.; Hendrickson, R. C.; Cloonan, S. M.; Gao, D.; Cross, J. R.; Vahdat, L. T.; Mittal, V. Copper depletion modulates mitochondrial oxidative phosphorylation to impair triple negative breast cancer metastasis. *Nature Communications* **2021**, *12*, 7311.

[8] Ishida, S.; Andreux, P.; Poitry-Yamate, C.; Auwerx, J.; Hanahan, D. Bioavailable copper modulates oxidative phosphorylation and growth of tumors. *Proceedings of the National Academy of Sciences of the United States of America* **2013**, *110*, 19507.

[9] Linder, M. C.; Moor, J. R.; Wright, K. Ceruloplasmin assays in diagnosis and treatment of human lung, breast, and gastrointestinal cancers. *Journal of the National Cancer Institute* **1981**, *67*, 263.

[10] Kahlson, M. A.; Dixon, S. J. Copper-induced cell death. *Science* **2022**, *375*, 1231.

[11] Chen, L.; Min, J.; Wang, F. Copper homeostasis and cuproptosis in health and disease. *Signal Transduction and Targeted Therapy* **2022**, *7*, 378.

[12] Ge, E. J.; Bush, A. I.; Casini, A.; Cobine, P. A.; Cross, J. R.; DeNicola, G. M.; Dou, Q. P.; Franz, K. J.; Gohil, V. M.; Gupta, S.; Kaler, S. G.; Lutsenko, S.; Mittal, V.; Petris, M. J.; Polishchuk, R.; Ralle, M.; Schilsky, M. L.; Tonks, N. K.; Vahdat, L. T.; Van Aelst, L.; Xi, D.; Yuan, P.; Brady, D. C.; Chang, C. J. Connecting copper and cancer: from transition metal signalling to metalloplasia. *Nature Reviews Cancer* **2022**, *22*, 102.

[13] Wu, W.; Yu, L.; Jiang, Q.; Huo, M.; Lin, H.; Wang, L.; Chen, Y.; Shi, J. Enhanced tumor-specific disulfiram chemotherapy by *in situ* Cu^{2+} chelation-initiated nontoxicity-to-toxicity transition. *Journal of the American Chemical Society* **2019**, *141*, 11531.

[14] Wu, W.; Yu, L.; Pu, Y.; Yao, H.; Chen, Y.; Shi, J. Copper-enriched prussian blue nanomedicine for *in situ* disulfiram toxification and photothermal antitumor amplification. *Advanced Materials* **2020**, *32*, 2000542.

[15] Meng, X.; Jia, K.; Sun, K.; Zhang, L.; Wang, Z. Smart responsive nanoplatform *via in situ* forming disulfiram-copper ion chelation complex for cancer combination chemotherapy. *Chemical Engineering Journal* **2021**, *415*, 128947.

[16] Shao, S.; Si, J.; Shen, Y. Copper as the Target for Anticancer Nanomedicine. *Advanced Therapeutics* **2019**, *2*, 1800147.

[17] Liu, W.; Xiang, H.; Tan, M.; Chen, Q.; Jiang, Q.; Yang, L.; Cao, Y.; Wang, Z.; Ran, H.; Chen, Y. Nanomedicine enables drug-potency activation with tumor sensitivity and hyperthermia synergy in the second near-infrared biowindow. *ACS Nano* **2021**, *15*, 6457.

[18] Chen, J.; Tan, X.; Huang, Y.; Xu, C.; Zeng, Z.; Shan, T.; Guan, Z.; Xu, X.; Huang, Z.; Zhao, C. Reactive oxygen species-activated self-amplifying prodrug nanoagent for tumor-specific Cu-chelate chemotherapy and cascaded photodynamic therapy. *Biomaterials* **2022**, *284*, 121513.

[19] Tsvetkov, P.; Coy, S.; Petrova, B.; Dreishpoon, M.; Verma, A.; Abdusamad, M.; Rossen, J.; Joesch-Cohen, L.; Humeidi, R.; Spangler Ryan, D.; Eaton John, K.; Frenkel, E.; Kocak, M.; Corsello Steven, M.; Lutsenko, S.; Kanarek, N.; Santagata, S.; Golub Todd, R. Copper induces cell death by targeting lipoylated TCA cycle proteins. *Science* **2022**, *375*, 1254.

[20] Brady, D. C.; Crowe, M. S.; Turski, M. L.; Hobbs, G. A.; Yao, X.; Chaikuad, A.; Knapp, S.; Xiao, K.; Campbell, S. L.; Thiele, D. J.; Counter, C. M. Copper is required for oncogenic BRAF signalling and tumorigenesis. *Nature* **2014**, *509*, 492.

[21] Pan, Q.; Rosenthal, D. T.; Bao, L.; Kleer, C. G.; Merajver, S. D. Antiangiogenic tetrathiomolybdate protects against Her2/neu-Induced breast carcinoma by hypoplastic remodeling of the mammary gland.

Chemical Science Accepted Manuscript

Clinical Cancer Research **2009**, *15*, 7441.

[22] Wang, J.; Luo, C.; Shan, C.; You, Q.; Lu, J.; Elf, S.; Zhou, Y.; Wen, Y.; Vinkenborg, J. L.; Fan, J.; Kang, H.; Lin, R.; Han, D.; Xie, Y.; Karpus, J.; Chen, S.; Ouyang, S.; Luan, C.; Zhang, N.; Ding, H.; Merkx, M.; Liu, H.; Chen, J.; Jiang, H.; He, C. Inhibition of human copper trafficking by a small molecule significantly attenuates cancer cell proliferation. *Nature Chemistry* **2015**, *7*, 968.

[23] Maiti, B. K.; J. G. Moura, J. Diverse biological roles of the tetrathiomolybdate anion. *Coordination Chemistry Reviews* **2021**, *429*, 213635.

[24] Hao, D.; Meng, Q.; Li, C.; Lu, S.; Xiang, X.; Pei, Q.; Jing, X.; Xie, Z. A paclitaxel prodrug with copper depletion for combined therapy toward triple-negative breast cancer. *ACS Nano* **2023**, *17*, 12383.

[25] Shao, S.; Zhou, Q.; Si, J.; Tang, J.; Liu, X.; Wang, M.; Gao, J.; Wang, K.; Xu, R.; Shen, Y. A non-cytotoxic dendrimer with innate and potent anticancer and anti-metastatic activities. *Nature Biomedical Engineering* **2017**, *1*, 745.

[26] Cui, L.; Gouw, A. M.; LaGory, E. L.; Guo, S.; Attarwala, N.; Tang, Y.; Qi, J.; Chen, Y.-S.; Gao, Z.; Casey, K. M.; Bazhin, A. A.; Chen, M.; Hu, L.; Xie, J.; Fang, M.; Zhang, C.; Zhu, Q.; Wang, Z.; Giaccia, A. J.; Gambhir, S. S.; Zhu, W.; Felsher, D. W.; Pegram, M. D.; Goun, E. A.; Le, A.; Rao, J. Mitochondrial copper depletion suppresses triple-negative breast cancer in mice. *Nature Biotechnology* **2021**, *39*, 357.

[27] Bano, S.; Raj, S. I.; Khalilullah, A.; Jaiswal, A.; Uddin, I. Selective and sensitive cation exchange reactions in the aqueous starch capped ZnS nanoparticles with tunable composition, band gap and color for the detection and estimation of Pb^{2+}, Cu^{2+} and Hg^{2+}. *Journal of Photochemistry and Photobiology A: Chemistry* **2021**, *405*, 112925.

[28] Goates, J. R.; Gordon, M. B.; Faux, N. D. Calculated values for the aolubility product constants of the metallic sulfides. *Journal of the American Chemical Society* **1952**, *74*, 835.

[29] Waggoner, W. H. The solubility product constants of the metallic sulfides. *Journal of Chemical Education* **1958**, *35*, 339.

[30] Zhang, J.; Yu, J.; Zhang, Y.; Li, Q.; Gong, J. R. J. N. l. Visible light photocatalytic H^2-production activity of CuS/ZnS porous nanosheets based on photoinduced interfacial charge transfer. *Nano Letters* **2011**, *11*, 4774.

[31] Yu, J.; Zhang, J.; Liu, S. Ion-exchange synthesis and enhanced visible-light photoactivity of CuS/ZnS nanocomposite hollow spheres. *The Journal of Physical Chemistry C* **2010**, *114*, 13642.

[32] Mondal, C.; Singh, A.; Sahoo, R.; Sasmal, A. K.; Negishi, Y.; Pal, T. Preformed ZnS nanoflower prompted evolution of CuS/ZnS p–n heterojunctions for exceptional visible-light driven photocatalytic activity. *New Journal of Chemistry* **2015**, *39*, 5628.

[33] Ravitz, S. F. The solubilities and free energies of some eetallic sulfides. *The Journal of Physical Chemistry* **1936**, *40*, 61.

[34] Zhao, X.; Zhao, K.; Su, J.; Sun, L. TiO2/CuS core-shell nanorod arrays with aging-induced photoelectric conversion enhancement effect. *Electrochemistry Communications* **2020**, *111*, 106648.

[35] Daskalakis, I.; Vamvasakis, I.; Papadas, I. T.; Tsatsos, S.; Choulis, S. A.; Kennou, S.; Armatas, G. S. Surface defect engineering of mesoporous Cu/ZnS nanocrystal-linked networks for improved visible-light photocatalytic hydrogen production. *Inorganic Chemistry Frontiers* **2020**, *7*, 4687.

[36] Zhai, S.; Abraham, A. M.; Chen, B.; Fan, Z.; Hu, J.; Cai, Z.; Thangadurai, V. Abundant Canadian pine with polysulfide redox mediating ZnS/CuS nanocomposite to attain high-capacity lithium sulfur battery. *Carbon* **2022**, *195*, 253.

[37] Shetty, A.; Mishra, S. K.; De, A.; Chandra, S. Smart releasing CuS/ZnS nanocomposite dual drug

carrier and photothermal agent for use as a theranostic tool for cancer therapy. *Journal of Drug Delivery Science and Technology* **2022**, *70*, 103252.

[38] Zhang, T.; Yan, B.; Zhang, L.; Yang, X. Ultrathin heterostructured ZnS/SnS2/CuS nanoflakes filled in N-doped carbon nanoboxes as novel cathode hosts for Li-SeS2 batteries. *Journal of Alloys and Compounds* **2024**, *990*, 174419.

[39] Li, K.; Xiong, H.; Wang, X.; Ma, Y.; Gao, T.-N.; Liu, Z.; Liu, Y.; Fan, M.; Zhang, L.; Song, S.; Qiao, Z.-A. Ligand-assisted coordinative self-assembly method to synthesize mesoporous ZnxCd1–xS nanospheres with nano-twin-induced phase junction for enhanced photocatalytic H^2 evolution. *Inorganic Chemistry* **2020**, *59*, 5063.

[40] Li, J.; Kessler, H.; Soulard, M.; Khouchaf, L.; Tuilier, M.-H. Nanosized zinc sulfide obtained in the presence of cationic surfactants. *Advanced Materials* **1998**, *10*, 946.

[41] Braun, P. V.; Osenar, P.; Stupp, S. I. Semiconducting superlattices templated by molecular assemblies. *Nature* **1996**, *380*, 325.

[42] Cheng, W.; Zeng, X.; Chen, H.; Li, Z.; Zeng, W.; Mei, L.; Zhao, Y. Versatile polydopamine platforms: synthesis and promising applications for surface modification and advanced nanomedicine. *ACS Nano* **2019**, *13*, 8537.

[43] Yang, P.; Zhu, F.; Zhang, Z.; Cheng, Y.; Wang, Z.; Li, Y. Stimuli-responsive polydopamine-based smart materials. *Chemical Society Reviews* **2021**, *50*, 8319.

[44] Tang, D.; Chen, X.; Kroemer, G. Cuproptosis: a copper-triggered modality of mitochondrial cell death. *Cell Research* **2022**, *32*, 417.

[45] Xu, C. F.; Liu, Y.; Shen, S.; Zhu, Y. H.; Wang, J. Targeting glucose uptake with siRNA-based nanomedicine for cancer therapy. *Biomaterials* **2015**, *51*, 1.

[46] Chen, W. H.; Luo, G. F.; Lei, Q.; Hong, S.; Qiu, W. X.; Liu, L. H.; Cheng, S. X.; Zhang, X. Z. Overcoming the heat endurance of tumor cells by interfering with the anaerobic glycolysis metabolism for improved photothermal therapy. *ACS Nano* **2017**, *11*, 1419.

[47] Wu, S.; Zhang, K.; Liang, Y.; Wei, Y.; An, J.; Wang, Y.; Yang, J.; Zhang, H.; Zhang, Z.; Liu, J.; Shi, J. Nano-enabled tumor systematic energy exhaustion *via* zinc (II) interference mediated glycolysis inhibition and specific GLUT1 depletion. *Advanced Science* **2022**, *9*, 2103534.

[48] Meng, Y.; Liu, P.; Zhou, W.; Ding, J.; Liu, J. Bioorthogonal DNA adsorption on polydopamine nanoparticles mediated by metal coordination for highly robust sensing in serum and siving cells. *ACS Nano* **2018**, *12*, 9070.

[49] Zandieh, M.; Liu, J. Transition metal-mediated DNA adsorption on dolydopamine nanoparticles. *Langmuir* **2020**, *36*, 3260.

[50] Denoyer, D.; Masaldan, S.; La Fontaine, S.; Cater, M. A. Targeting copper in cancer therapy: 'Copper That Cancer'. *Metallomics* **2015**, *7*, 1459.

[51] Yang, Y.; Li, M.; Chen, G.; Liu, S.; Guo, H.; Dong, X.; Wang, K.; Geng, H.; Jiang, J.; Li, X. Dissecting copper biology and cancer treatment: 'Activating Cuproptosis or suppressing Cuproplasia'. *Coordination Chemistry Reviews* **2023**, *495*, 215395.

[52] Gupte, A.; Mumper, R. J. Elevated copper and oxidative stress in cancer cells as a target for cancer treatment. *Cancer Treatment Reviews* **2009**, *35*, 32.

[53] Harvey, L. J.; Ashton, K.; Hooper, L.; Casgrain, A.; Fairweather-Tait, S. J. Methods of assessment of copper status in humans: a systematic review. *American Journal of Clinical Nutrition* **2009**, *89*, 2009.

[54] Linder, M. C. Ceruloplasmin and other copper binding components of blood plasma and their functions: an update. *Metallomics* **2016**, *8*, 887.

[55] Wang, J.; Luo, C.; Shan, C.; You, Q.; Lu, J.; Elf, S.; Zhou, Y.; Wen, Y.; Vinkenborg, J. L.; Fan, J.; Kang, H.; Lin, R.; Han, D.; Xie, Y.; Karpus, J.; Chen, S.; Ouyang, S.; Luan, C.; Zhang, N.; Ding, H.; Merkx, M.; Liu, H.; Chen, J.; Jiang, H.; He, C. Inhibition of human copper trafficking by a small molecule significantly attenuates cancer cell proliferation. *Nature Chemistry* **2015**, *7*, 968.

[56] Arami, H.; Khandhar, A.; Liggitt, D.; Krishnan, K. M. In vivo delivery, pharmacokinetics, biodistribution and toxicity of iron oxide nanoparticles. *Chemical Society Reviews* **2015**, *44*, 8576.

[57] Kumar, M.; Kulkarni, P.; Liu, S.; Chemuturi, N.; Shah, D. K. Nanoparticle biodistribution coefficients: A quantitative approach for understanding the tissue distribution of nanoparticles. *Advanced Drug Delivery Reviews* **2023**, *194*, 114708.

[58] Mao, X.; Schimmer, A. D. The toxicology of Clioquinol. *Toxicology Letters* **2008**, *182*, 1.

[59] Huang, J.; Campian, J. L.; Gujar, A. D.; Tran, D. D.; Lockhart, A. C.; DeWees, T. A.; Tsien, C. I.; Kim, A. H. A phase I study to repurpose disulfiram in combination with temozolomide to treat newly diagnosed glioblastoma after chemoradiotherapy. *Journal of Neuro-Oncology* **2016**, *128*, 259.

[60] Ford, E. S. Serum copper concentration and coronary heart disease among US adults. *American Journal of Epidemiology* **2000**, *151*, 1182.

[61] Walshe, J. M. Penicillamine, a new oral therapy for Wilson's disease. *The American Journal of Medicine* **1956**, *21*, 487.

[62] Bandmann, O.; Weiss, K. H.; Kaler, S. G. Wilson's disease and other neurological copper disorders. *The Lancet Neurology* **2015**, *14*, 103.

[63] Brewer, G. J.; Dick, R. D.; Grover, D. K.; LeClaire, V.; Tseng, M.; Wicha, M.; Pienta, K.; Redman, B. G.; Jahan, T.; Sondak, V. K.; Strawderman, M.; LeCarpentier, G.; Merajver, S. D. Treatment of metastatic cancer with tetrathiomolybdate, an anticopper, antiangiogenic agent: Phase I study. *Clinical Cancer Research* **2000**, *6*, 1.

[64] Weiss, K. H.; Askari, F. K.; Czlonkowska, A.; Ferenci, P.; Bronstein, J. M.; Bega, D.; Ala, A.; Nicholl, D.; Flint, S.; Olsson, L.; Plitz, T.; Bjartmar, C.; Schilsky, M. L. Bis-choline tetrathiomolybdate in patients with Wilson's disease: an open-label, multicentre, phase 2 study. *The Lancet Gastroenterology & Hepatology* **2017**, *2*, 869.

Chemical Science Accepted Manuscript

Data supporting this study is available in the ESI and further details are available from the authors on reasonable request.

Chemical Science Accepted Manuscript